JCTC Journal of Chemical Theory and Computation

Article

pubs.acs.org/JCTC

Evaluation of the Linear and Second-Order NLO Properties of Molecular Crystals within the Local Field Theory: Electron Correlation Effects, Choice of XC Functional, ZPVA Contributions, and Impact of the Geometry in the Case of 2-Methyl-4-nitroaniline

Tomasz Seidler,*[,†,‡] Katarzyna Stadnicka,[†] and Benoît Champagne*[,‡]

[†]Faculty of Chemistry, Jagiellonian University, ul, Ingardena 3, 30-060, Kraków, Poland

[‡]Laboratoire de Chimie Théorique, Unité de Chimie Physique Théorique et Structurale, University of Namur, rue de Bruxelles, 61, B-5000, Namur, Belgium

Supporting Information

ABSTRACT: The linear [$\chi^{(1)}$] and second-order nonlinear [$\chi^{(2)}$] optical susceptibilities of the 2-methyl-4-nitroaniline (MNA) crystal are calculated within the local field theory, which consists of first computing the molecular properties, accounting for the dressing effects of the surroundings, and then taking into account the local field effects. Several aspects of these calculations are tackled with the aim of monitoring the convergence of the $\chi^{(1)}$ and $\chi^{(2)}$ predictions with respect to experiment by accounting for the effects of (i) the dressing field within successive approximations, of (ii) the first-order ZPVA corrections, and of (iii) the geometry. With respect to the reference CCSD-based results, besides double hybrid functionals, the most reliable exchange-correlation functionals are LC-BLYP for the static $\chi^{(1)}$ and CAM-B3LYP (and M05-2X, to a lesser extent) for the dynamic $\chi^{(1)}$ but they strongly underestimate $\chi^{(2)}$. Double hybrids perform better for $\chi^{(2)}$ but not necessarily for $\chi^{(1)}$, and, moreover, their performances are much similar to MP2, which is known to slightly overestimate β, with respect to high-level coupled-clusters calculations and, therefore, $\chi^{(2)}$. Other XC functionals with less HF exchange perform poorly with overestimations/underestimations of $\chi^{(1)}/\chi^{(2)}$, whereas the HF method leads to underestimations of both. The first-order ZPVA corrections, estimated at the B3LYP level, are usually small but not negligible. Indeed, after ZPVA corrections, the molecular polarizabilities and first hyperpolarizabilities increase by 2% and 5%, respectively, whereas their impact is magnified on the macroscopic responses with enhancements of $\chi^{(1)}$ by up to 5% and of $\chi^{(2)}$ by as much as 10%−12% at λ = 1064 nm. The geometry plays also a key role in view of predicting accurate susceptibilities, particularly for push−pull π-conjugated compounds such as MNA. So, the geometry optimized using periodic boundary conditions is characterized by an overestimated bond length alternation, which gives larger molecular properties and even larger macroscopic responses, because of the local field factor amplification effects. Our best estimates based on experimental geometries, charge dressing field, ZPVA correction, and CCSD molecular properties lead to an overestimation of $\chi^{(1)}$ by 12% in the static limit and 7% at λ = 1064 nm. For $\chi^{(2)}$, the difference, with respect to the experiment, is satisfactory and of the order of one standard deviation.

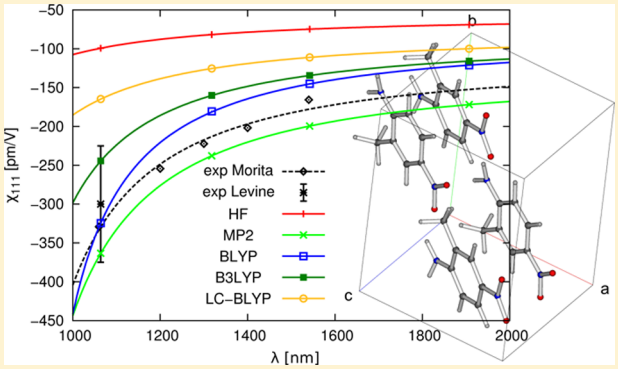

1. INTRODUCTION

Molecular crystals presenting second-order nonlinear optical (NLO) responses are of interest for telecommunication and data storage applications. The optimization of these responses results from a multidisciplinary approach that combines the design and preparation of materials, and their optical and physicochemical characterizations, together with quantum-chemical calculations, because of their predictive and interpretative potential.[1−6] The assumption of zero overlap between the molecules constitutive of the crystals—valid to a large extent—allows the use of a range of methods correlating the isolated molecules properties with their macroscopic counterparts and vice versa. Indeed, on the one hand, measurements of the electric susceptibilities through the refractive indices (linear) and second harmonic (SH) intensities give an insight into the molecular properties such as the polarizability (α) and the first hyperpolarizability (β). So, the anisotropic Lorentz field factor approximation (ALFFA) has been used as one of the first approximations[7,8] to extract β from $\chi^{(2)}$ values. Later on, it was used to estimate $\chi^{(2)}$ from β. An improvement to ALFFA was brought by the Rigorous Local Field Theory (RLFT), due to Munn and co-workers.[9,10] This approach, which has already been tested extensively, allows for

Received: February 25, 2014
Published: April 1, 2014

   dx.doi.org/10.1021/ct5001654 | J. Chem. Theory Comput. 2014, 10, 2114−2124

the inclusion of in-crystal polarization.[11,12] These dressing effects are of primary importance in the case of polar molecules, which themselves consist of a source of electron density polarization of the surroundings. In our recent proposition,[13] dressing effects are accounted for by embedding the molecule in a network of point charges and, subsequently, the RLFT scheme is used to get the crystal properties. This scheme allows one to reflect the nonuniformity of the dressing field and provides results in good agreement with experimental data. However, several aspects related to predicting the linear and nonlinear optical susceptibilities must still be addressed, including the following: (i) the choice of exchange-correlation (XC) functional;[14−24] (ii) the importance of the zero-point vibrational averaging correction (ZPVA),[25−31] especially at optical frequencies, since, so far, the crystal susceptibility calculations have been based on molecular electronic (hyper)-polarizabilities; (iii) the impact of the geometry; and (iv) the description of frequency dispersion.[32−35] These different effects are crucial on the hyperpolarizabilities of isolated molecules, as well as molecules in solution, and they have already been studied for small molecules as well as for push−pull π-conjugated molecules; however, here, we focus on their impact on the targeted crystal linear and second-order nonlinear susceptibilities. The paper is organized as follows. Section 2 summarizes (i) the main RLFT equations to determine the crystal susceptibilities from the molecular responses and (ii) the computational approach to evaluate the molecular responses by including electron correlation, frequency dispersion, and ZPVA corrections. Section 3 presents and discusses the results before conclusions are drawn in Section 4.

2. THEORETICAL METHODS AND COMPUTATIONAL DETAILS

2.1. The Electrostatic Interaction Scheme. In order to find a connection between the macroscopic electric properties of matter ($\chi^{(1)}$, $\chi^{(2)}$) and their molecular analogues (α, β), one must define a relationship between the macroscopic electric field ($\underline{E}$) and the local electric field ($\underline{F}$). A linear transformation form can be assumed:

$$\underline{F}_k = \underline{\underline{d}}_k \cdot \underline{E} \tag{1}$$

where k stands for the molecules or submolecules of the reference unit cell and $\underline{\underline{d}}$ is the local field tensor. In isotropic situations, this tensor is simplified to a scalar quantity of 1/3, because of rotational averaging. An efficient approach to calculate the $\underline{\underline{d}}$ tensor, which was developed by Hurst and Munn[10,36] and called RLFT, is based on the electrostatic interaction scheme in the electric dipole approximation. In this method, the polarizable molecules located in the crystal lattice screening the external field are treated explicitly. A self-consistent set of equations is solved in the reciprocal space, because of the Fourier transformation properties, yielding an expression of the local field tensor under the form

$$\underline{\underline{d}}_k(\omega) = \sum_{k'} \underline{\underline{D}}_{kk'}(\omega) = \sum_{k'} \left[\underline{\underline{1}} - \frac{1}{V\varepsilon_0} \underline{\underline{\alpha}}(\omega) \cdot \underline{\underline{L}} \right]^{-1}_{kk'} \tag{2}$$

where V is the unit cell volume, ε_0 the dielectric permittivity of vacuum, $\underline{\underline{\alpha}}$ a block-diagonal supermatrix of the (sub)molecules polarizabilities, and $\underline{\underline{L}}$ the dipole−dipole Lorentz tensor. Then, the linear and second-order nonlinear electric susceptibility tensors are calculated with aid of the following relations:[37]

$$\underline{\underline{\chi}}^{(1)}(\omega) = \frac{1}{V\varepsilon_0} \sum_k \underline{\underline{\alpha}}_k(\omega) \cdot \underline{\underline{d}}_k(\omega) \tag{3}$$

$$\underline{\underline{\chi}}^{(2)}(-2\omega;\, \omega,\, \omega) = \frac{1}{2V\varepsilon_0} \sum_k \underline{\underline{d}}_k^{\mathrm{T}}(2\omega) \cdot \underline{\underline{\underline{\beta}}}_k(-2\omega;\, \omega,\, \omega) \vdots\, \underline{\underline{d}}_k(\omega) \underline{\underline{d}}_k(\omega) \tag{4}$$

where $\underline{\underline{\alpha}}_k$ and $\underline{\underline{\underline{\beta}}}_k$ are the polarizability and first hyperpolarizability tensors of the kth (sub)molecule in the unit cell, and the rest of the symbols have already been explained. This method enables also the calculation of the uniform polarizing electric field originating from the point dipoles of the surrounding molecules

$$\underline{F}_{k0} = \frac{1}{V\varepsilon_0} \sum_{k'k''} \underline{\underline{D}}_{kk'}(\omega = 0) \cdot \underline{\underline{L}}_{k'k''} \cdot \underline{p}_{k''0} \tag{5}$$

where $\underline{p}_{k0}$ is the permanent dipole moment of the kth (sub)molecule in the unit cell. However, this method tends to overestimate the *in-crystal* molecular response.[13] On the other hand, a point charge field can describe the nonuniformity of the electric field more accurately than the molecular dipoles. In this study, although other definitions of charges could be employed, including electrostatic potential (ESP) derived charges, the point charges are chosen as the Mulliken charges determined from periodic B3LYP calculations. In our previous work,[13] the impact of varying the atomic Mulliken charges by ±5% was studied for $\chi^{(1)}$ and $\chi^{(2)}$ of MNA. It amounts to less than 1%−2% for the linear responses and to 5% for second-order responses. When performing the molecular electric properties calculations, they are located spherically around the reference molecule.

The so-called RLFTn partitioning scheme is used throughout the paper. Here, n stands for the number of heavy (non-hydrogen) atoms while the hydrogen atoms belong to the submolecule of the corresponding heavy atom to which they are attached/bonded.

2.2. Calculations of the Molecular Properties and Computational Details. Two main sets of geometries were employed in this study. The first one is the experimental geometry taken from ref 38. It is an outcome of a thorough combination of high-resolution X-ray (charge density) and neutron diffraction experiments. The second one is the result of a periodic boundary conditions B3LYP/6-31G(d,p) optimization as implemented in CRYSTAL09[39,40] and has been taken from ref 13. An additional geometry optimization was performed in the point charge field for a single molecule at the B3LYP/6-311++G(d,p) level of theory (starting from the experimental geometry). This optimization was followed by the calculations of the harmonic frequencies and of the ZPVA corrections.

The molecular properties (α, β) were evaluated at different levels of approximation. The reference correlated properties were obtained with the MP2 and MP4-SDQ methods using the 6-311++G(d,p) basis set. At the density functional theory (DFT) level, several exchange-correlation functionals were employed. These can be divided into five distinct groups: generalized gradient approximation (GGA) (represented by BLYP), hybrid GGA (represented by B3LYP and B98), long-range corrected (represented by LC-BLYP and CAM-B3LYP), hybrid meta-GGA (represented by M05 and M05-2X), and

dx.doi.org/10.1021/ct5001654 | J. Chem. Theory Comput. 2014, 10, 2114−2124

double hybrid (represented by B2PLYP and mPW2PLYP). Additional values were also obtained at the Hartree−Fock level. The 6-311++G(3df,3pd) basis set was used for all the functionals except for the last two, for which the 6-311++G(d,p) basis set was used. These single-molecule calculations were performed with the Gaussian 09.[41] Frequency dispersion at the MP2, MP4, B2PLYP, and mPW2PLYP levels was introduced using the simplified multiplicative scheme with aid of the TD-B3LYP method.[13,42] At the HF level and at the DFT level, using all but the double hybrid XC functionals, dynamic α and β values were obtained using analytical response approaches,[43] whereas at the MP2, MP4, B2PLYP, and mPW2PLYP levels the static quantities were determined using the finite field scheme. Field amplitudes ranging from 0.001 a.u. to 0.003 a.u. were employed to ensure high numerical accuracy on the derivatives. Moreover, the Dalton2011 package[44,45] was used to calculate the frequency-dependent CCSD/6-31++G(d,p) properties. For technical reasons, the charge field could not be accounted for at the latter level and, instead, the polarizing field was described by the electric dipole field. In order to estimate approximate CCSD values with charge field, another simple multiplicative correction that relied on MP2 results was adopted:

$$\chi_{\mathrm{chf}}^{\mathrm{CCSD}} \simeq \chi_{\mathrm{dipf}}^{\mathrm{CCSD}} \times \frac{\chi_{\mathrm{chf}}^{\mathrm{MP2}}}{\chi_{\mathrm{dipf}}^{\mathrm{MP2}}} \tag{6}$$

where the subscripts "chf" and "dipf" stand for charge and dipole polarizing field in the molecular calculations, respectively. The modified results are marked as CCSD*.

The first-order ZPVA corrections to the molecular electric properties (P) were calculated, using the B3LYP XC functional, according to the following expression:[25]

$$P^{\mathrm{ZPVA}} = \frac{\hbar}{4}\sum_{a}^{3N-6}\frac{\partial^2 P/\partial^2 Q_a}{\omega_a} - \frac{\hbar}{4}\sum_{a}^{3N-6}\sum_{b}^{3N-6}\frac{F_{abb}}{\omega_b}\frac{\partial P/\partial Q_a}{\omega_a^2} \tag{7}$$

where Q_a and ω_a stand for the vibrational normal coordinate and frequency of the ath harmonic mode and F_{abb} is a cubic force constant matrix element. The evaluations of the first-order derivatives of the Hessian matrix and the first- and second-order derivatives of the properties, with respect to the normal mode coordinates, were carried out using the finite distortion method at equilibrium geometry. A distortion step size of 0.05 a.u. was used. The normal modes were visualized using the pyVib2 program.[46]

$\chi^{(2)}$ $(-2\omega;\omega,\omega)$ tensor elements are reported in the eigenbasis of the $\chi^{(1)}$ $(-\omega;\omega)$ tensor, while indices 1, 2, and 3 refer to the abc* system for the $\chi^{(1)}$ tensor.

3. RESULTS

3.1. Effects of Electron Correlation and the Choice of XC Functional on $\chi^{(1)}$ and $\chi^{(2)}$. The molecule of MNA is sketched in Figure 1. In a first step, the dressed molecular properties are calculated for both the experimental and periodic boundary conditions geometries. To get the charge fields, the Mulliken charges are calculated for both geometries and are compared in Table S1 (Supporting Information). For the experimental geometry, the convergence of the charge electric field at the center of nuclear charges of the molecule is presented in Table 1 (that for the other geometry was given in ref 13). A cutting radius of 160 Å is found to be suitable to achieve convergence, as for the optimized geometry. The optimized geometry leads to an increase of the polarizing field of the order of ca. 2.5%. This effect will be discussed in more details in Section 3.3. The static ($\lambda = \infty$) and dynamic (λ = 1064 nm) molecular polarizabilities and hyperpolarizabilities calculated for the experimental geometry with inclusion of the charge embedding field are presented in Tables S2 and S3 (Supporting Information), respectively. All but the double hybrid functionals give strong underestimations of the β tensor components, with respect to the correlated methods. The most severe underestimations are observed for the BLYP functional in the $\lambda = \infty$ limit. On the other hand this functional gives the largest α values. These results are consistent with early works on push−pull π-conjugated systems,[14,15] showing that GGA and hybrid GGA functionals overestimate/underestimate the polarizability/first hyperpolarizability in small compounds like p-nitroaniline while they overestimate both linear and nonlinear responses in the case of large compounds. As we will see later, these opposite effects of the XC functionals on α and β lead to overestimations of $\chi^{(1)}$, whereas for $\chi^{(2)}$, the situation is more contrasted, since the polarizability enters three times in eq 4 via the local field tensor components.

The CCSD tensor values are larger than the corresponding MP2 and MP4 results, because of the use of the uniform dipole polarizing field whereas the MP2 and MP4 results are obtained with the charge field. It will be shown later that an approximate scaling leads to reasonable electric susceptibility tensor components. The details of the dressed dipoles and dipole fields are supplemented in Table S4 in the Supporting Information for the MP2 and CCSD levels. The CCSD values differ by 1% or less, with respect to the MP2 results,

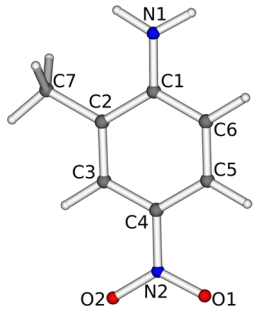

Figure 1. Atom numbering scheme of MNA.

Table 1. Convergence of the Electric Field (in GV/m) as a Function of R_{cut} at the Center of Nuclear Charge for the First MNA Molecule of the Unit Cell within the abc* Crystal System[a]

R_{cut} (Å)	F_x	F_y	F_z	$\lvert F\rvert$
20	−2.84	0.49	−1.41	3.21
40	−3.64	0.74	−1.14	3.89
60	−2.96	0.64	−1.35	3.32
80	−2.85	0.67	−1.33	3.21
100	−3.03	0.83	−1.32	3.41
120	−3.12	1.05	−1.23	3.51
140	−3.12	0.59	−1.30	3.43
160	−3.12	0.72	−1.27	3.44
180	−3.25	0.76	−1.30	3.58
200	−3.21	0.73	−1.14	3.48

[a]The Mulliken atomic charges were obtained at the B3LYP/6-31G(d,p) level using periodic boundary conditions.

dx.doi.org/10.1021/ct5001654 | J. Chem. Theory Comput. 2014, 10, 2114−2124

Table 2. Influence of the Method Used for Calculating the Static ($\lambda = \infty$) Molecular Properties on the Macroscopic Electric Properties Taking into Account the Dressing Charge Electric Field (Experimental Geometry)[a]

method	$\chi^{(1)}_{11}$	$\chi^{(1)}_{22}$	$\chi^{(1)}_{33}$	$\chi^{(1)}_{13}$	n_x	n_y	n_z	$\chi^{(2)}_{111}$	$\chi^{(2)}_{122} = \chi^{(2)}_{212}$
experiment	2.453[b]	1.956[b]	1.422[b]	0.709[b]	1.953[b]	1.719[b]	1.436[b]	117.8[c]	
HF	2.295	1.797	1.385	0.609	1.898	1.672	1.442	−60.0	−2.1
MP2	2.657	1.931	1.421	0.807	1.898	1.672	1.442	−134.3	−11.4
MP4	2.453	1.853	1.355	0.716	1.951	1.689	1.415	−108.7	−8.5
CCSD	2.754	1.926	1.426	0.866	2.045	1.710	1.414	−180.0	−15.2
CCSD*	2.682	1.948	1.471	0.798	2.019	1.717	1.440	−143.8	−11.6
BLYP	3.039	2.067	1.631	0.936	2.123	1.751	1.471	−91.0	−5.0
B3LYP	2.835	1.982	1.550	0.853	2.064	1.727	1.457	−90.8	−5.2
B98	2.800	1.971	1.539	0.837	2.054	1.724	1.456	−88.2	−5.1
LC-BLYP	2.499	1.882	1.434	0.705	1.962	1.698	1.443	−83.1	−5.4
CAM-B3LYP	2.664	1.937	1.498	0.774	2.012	1.714	1.453	−88.3	−5.4
M05	2.826	1.992	1.539	0.852	2.061	1.730	1.454	−89.1	−5.0
M05-2X	2.591	1.889	1.466	0.747	1.991	1.700	1.447	−80.5	−4.6
B2PLYP	2.742	1.903	1.441	0.853	2.041	1.704	1.421	−123.1	−8.9
mPW2PLYP	2.703	1.892	1.431	0.834	2.029	1.701	1.420	−118.2	−8.4

[a]CCSD results are obtained with uniform dipole dressing field while CCSD* stands for simulated dressing electric field according to eq 6 (see Section 2.2). $\chi^{(2)}$ tensor elements given in units of pm/V. [b]Data taken from ref 61 ($\angle(a,x) = 27°$). [c]Data extrapolated to $\lambda = \infty$, from ref 62.

Table 3. Influence of the Method Used To Calculate the Dynamic (λ = 1064 nm) Molecular Properties on the Macroscopic Electric Properties Taking into Account the Dressing Electric Field (Experimental Geometry)[a]

method	$\chi^{(1)}_{11}$	$\chi^{(1)}_{22}$	$\chi^{(1)}_{33}$	$\chi^{(1)}_{13}$	n_x	n_y	n_z	$\chi^{(2)}_{111}$	$\chi^{(2)}_{122}$	$\chi^{(2)}_{212}$
experiment	2.804[b]	2.000[b]	1.521[b]	0.883[b]	2.063[b]	1.732[b]	1.439[b]	300(75)[c]	45(11)[c]	
HF	2.391	1.833	1.416	0.652	1.928	1.683	1.445	−99.3	−2.9	−5.2
MP2	2.865	1.983	1.479	0.904	2.076	1.727	1.426	−363.3	−29.4	−26.6
MP4	2.637	1.901	1.407	0.802	2.008	1.703	1.418	−286.3	−21.4	−19.7
CCSD	2.967	1.983	1.485	0.966	2.108	1.727	1.417	−438.2	−32.8	−35.9
CCSD*	2.857	2.002	1.522	0.880	2.072	1.733	1.444	−319.0	−23.1	−26.1
BLYP	3.332	2.137	1.713	1.075	2.206	1.771	1.475	−324.5	−12.1	−20.3
B3LYP	3.059	2.041	1.613	0.959	2.130	1.744	1.461	−244.5	−10.9	−16.5
B98	3.011	2.028	1.599	0.937	2.116	1.740	1.460	−226.9	−10.4	−15.4
LC-BLYP	2.637	1.928	1.475	0.768	2.005	1.711	1.447	−164.8	−9.6	−12.4
CAM-B3LYP	2.838	1.989	1.549	0.855	2.065	1.729	1.457	−198.4	−10.5	−14.3
M05	3.037	2.050	1.600	0.951	2.124	1.747	1.458	−230.7	−10.3	−15.7
M05-2X	2.749	1.937	1.513	0.821	2.039	1.714	1.450	−171.0	−8.6	−12.0
B2PLYP	2.962	1.953	1.502	0.957	2.106	1.719	1.424	−337.3	−23.1	−21.1
mPW2PLYP	2.917	1.942	1.491	0.935	2.093	1.715	1.424	−322.0	−21.6	−19.8

[a]CCSD results are obtained with uniform dipole dressing field, while CCSD* stands for simulated dressing electric field according to eq 6 (see Section 2.2). $\chi^{(2)}$ tensor elements are given in units of pm/V. [b]Data taken from ref 61 ($\angle(a,x) = 27°$). [c]Data taken from ref 63.

substantiating, to a large extent, the subsequent use of eq 6. The angle between the charge and dipole field is ca. 19° and the dipole field amplitude is ca. 50% larger than that of the charge field. This is expected to overestimate the molecular and therefore the macroscopic properties, as recently observed.[13] These overestimations will be corrected using eq 6.

The static and dynamic (λ = 1064 nm) electric susceptibility tensor components are listed in Tables 2 and 3, respectively. To facilitate the following discussion, the deviations of the $\chi^{(1)}$ and $\chi^{(2)}_{111}$ tensor components, with respect to experiment, ($\chi_{calc} - \chi_{exp}$), are presented in Figures 2 and 3. The first observation is that none of the methods is able to reproduce satisfactorily all the experimental results in the $\lambda = \infty$ limit. The closest agreement for a wave function correlated method is achieved with the MP4 method, although slight underestimations are clear. MP2 and CCSD* results are very close to each other and give small overestimations of the $\chi^{(1)}_{11}$ and $\chi^{(2)}_{111}$. On the other hand, the HF gives the lowest bounds for all but the $\chi^{(1)}_{33}$ tensor component, which was attained with MP4. At λ = 1064 nm, the results are slightly different with the best agreement achieved with the MP2 and CCSD* methods while the MP4 underestimations are larger than in the $\lambda = \infty$ limit. These observations result from the limitations of B3LYP (and CCSD) to describe the frequency dispersion, from the underestimations of the static limit values (vide supra), from the lack of ZPVA contributions, and also from possible imprecisions or inaccuracies on the measurements, that cannot be excluded.

The XC functionals, interestingly, behave in a consistent fashion, following the percentage of exact Hartree−Fock exchange. The pure GGA functional (BLYP)[47,48] gives the largest overestimations of the $\chi^{(1)}$ tensor components for both the $\lambda = \infty$ and λ = 1064 nm cases. Then, although β is underestimated, an overestimated (frequency dispersion of the) $\chi^{(1)}$ tensor components leads to a very strong $\chi^{(2)}_{111}$ frequency dispersion, so that BLYP underestimates the static $\chi^{(2)}_{111}$ but overestimates it at λ = 1064 nm. The use of hybrid functionals with exact exchange content of ca. 20% (B3LYP[47,49] and B98[50]) as well as hybrid meta-GGA M05[51] (with 27% of the HF

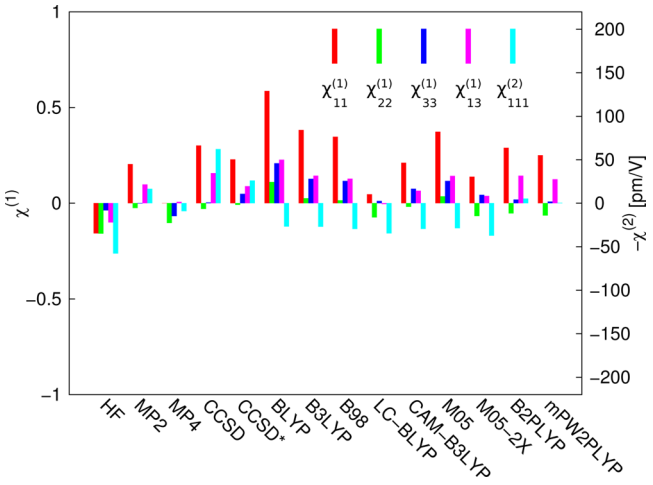

Figure 2. Differences with respect to experiment for selected electric susceptibility tensor components ($\lambda = \infty$) taking into account the dressing charge electric field (experimental geometry).

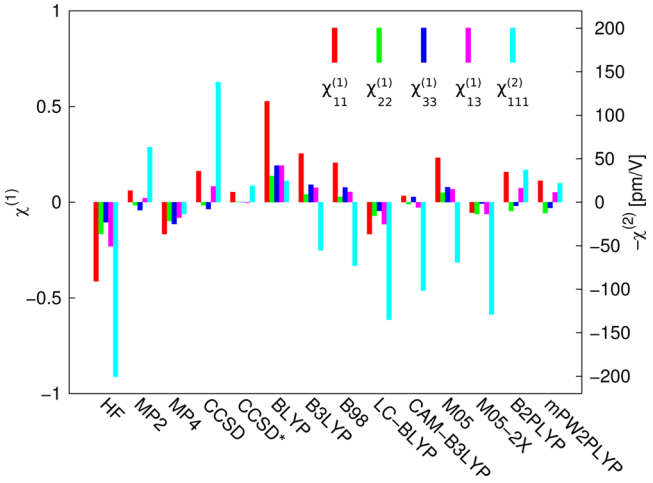

Figure 3. Differences with respect to experiment for selected electric susceptibility tensor components (λ = 1064 nm) taking into account the dressing charge electric field (experimental geometry).

exchange) leads to smaller α and $\chi^{(1)}$ tensor components, but the corrections are too small and the $\chi^{(1)}$ tensor components remain overestimated. Although the calculated frequency dispersion obtained using these methods is among the strongest of all the functionals used (after BLYP), the agreement with experiment for the dynamic $\chi^{(1)}$ quantities is better than in the static limit, the overestimations being reduced. Using hybrid GGA and meta-GGA functionals all $\chi^{(2)}_{111}$ values display underestimations, although the values at λ = 1064 nm fall within the experimental value minus one standard deviation.

In the next class of functionals, the amount of HF exchange gets larger: in LC-BLYP[52] and CAM-B3LYP,[53] the amount of exact exchange depends on the distance and, for large distances, tends to 100% and 65%, respectively, whereas in M05-2X,[54] it amounts to 54% (i.e., twice as much as that in M05). These functionals perform quite well, especially LC-BLYP in the static limit and CAM-B3LYP at λ = 1064 nm. This is in agreement with the results found in ref 23 for small molecules and in ref 55 for π-conjugated systems. The use of CAM-B3LYP reduces the overestimations on $\chi^{(1)}$ obtained with the B3LYP functional. Interestingly, this functional yields the best agreement with experimental $\chi^{(1)}$ results at λ = 1064 nm, more probably as a result of error compensations. In the static limit, the performance of these range-separated hybrids is similar to that of the hybrids and GGAs to predict $\chi^{(2)}_{111}$. On the other hand, the $\chi^{(2)}_{111}$ frequency dispersion obtained with these methods is even weaker than with hybrid functionals and, thus, even more insufficient. This is evidenced by the $\chi^{(2)}_{111}$ amplitudes, which are below the experimental value minus two standard deviations.

The most sophisticated double hybrid functionals, B2-PLYP[56] and mPW2PLYP,[57] which incorporate an additional MP2 correlation contribution yield results very close to the true MP2 method, for both $\chi^{(1)}$ and $\chi^{(2)}$. The $\chi^{(1)}$ results are slightly larger—and, therefore, slightly overestimated—than those at the MP2 level. For both the static and dynamic $\chi^{(2)}_{111}$, the performance of these double hybrids is similar to that of MP4 and CCSD* and better than that of the other XC functionals.

3.2. ZPVA Correction on the Molecular Properties.

The amplitude of the first-order ZPVA corrections to the molecular properties has been estimated for both the isolated molecule and the molecule dressed by the charge field. The geometry optimization in the dressing field of point charges was performed starting from the experimental parameters with the same R_{cut} = 160 Å as for the aforementioned properties calculations. The final set of optimized bond lengths is presented (together with those obtained with other methods) in Table 4. The charge-embedded optimized geometries reproduce very well the experimental data, including the BLA (0.031 Å), with an accuracy overcoming the PBC results.

Table 4. Selected Bond Lengths (in Å) of MNA Molecule Optimized with Different Methods in Comparison with Experimental Data

	Bond Length (Å)			
	B3LYP/6-31G**		B3LYP/6-311++G**	
bond	experiment[a]	with PBC[b]	isolated (no field)[b]	with charge field
C1C2	1.422	1.430	1.418	1.426
C2C3	1.385	1.383	1.388	1.384
C3C4	1.401	1.408	1.395	1.403
C4C5	1.399	1.406	1.393	1.402
C5C6	1.379	1.376	1.383	1.379
C6C1	1.416	1.422	1.407	1.418
C1N1	1.357	1.355	1.380	1.364
C2C7	1.502	1.505	1.507	1.507
C4N2	1.430	1.420	1.462	1.422

[a]Data taken from ref 38. [b]Data taken from ref 13.

The presence of the charge dressing field also modifies the vibrational frequencies, in particular the lowest ones, corresponding to large out-of-plane motions and internal rotations that are more impacted by the surrounding than the skeleton distortions (see Table S5 in the Supporting Information). A comparison of the molecular properties calculated without and with the ZPVA correction is given in Tables S2 and S3 in the Supporting Information (entries B3LYPa and B3LYPb)). Using the B3LYP XC functional, the first-order $\Delta\alpha^{ZPVA}$ correction amounts to ~2% of both the static and dynamic polarizabilities, while the situation is more complex for the first hyperpolarizability, because $\Delta\beta^{ZPVA}_{tot}$ varies with the frequency. In the static limit, it slightly reduces β_{tot},

whereas at λ = 1064 nm, the ZPVA correction enhances β_{tot} by 5%. A complementary look at this frequency dispersion effect is provided by analyzing $\beta_{\parallel}$ and the contributions of the different normal modes (see Table S5 in the Supporting Information). When no polarizing electric field is present, the ZPVA contribution to $\beta_{\parallel}$ is negative at $\lambda = \infty$ and λ = 1907 nm, but it changes sign between λ = 1907 nm and λ = 1064 nm. The vibrational modes that exhibit dominant mechanical anharmonicity ZPVA corrections correspond to totally symmetric *p*NA modes, which is consistent with the results of ref 26. The mechanical and electrical contributions to the total $\Delta\beta_{\parallel}^{ZPVA}$ are of opposite signs for the wavelength range going from $\lambda = \infty$ to λ = 1064 nm. For both contributions, the frequency dispersions are quite large, going in opposite directions if considering their amplitudes, which explains why (i) the total $\Delta\beta_{\parallel}^{ZPVA}$ changes sign by going from λ = 1907 nm to λ = 1064 nm and (ii) its amplitude strongly increases. When accounting for the dressing field, the mechanical anharmonicity contribution to $\Delta\beta_{\parallel}^{ZPVA}$ evolves with the frequency in a similar way to the case of the undressed properties. The situation changes for the electrical anharmonicity counterpart that becomes large and positive at λ = 1064 nm, so that $\Delta\beta_{\parallel}^{ZPVA}$ is four times larger than for the isolated molecule and it amounts to 5% of the electronic β_{tot}, estimated at the same level of approximation. The most contributing modes to ZPVA are sketched in Figure 4. They are similar no matter whether the charge field is taken into account or not. For modes 8/9 (CN, NO_2, and NH_2 stretchings) and 23 (ring breathing), the mechanical anharmonicity dominates and brings a positive contribution to $\Delta\beta_{\parallel}^{ZPVA}$. On the other hand, for modes 18 (NO_2 out-of-plane deformation), 32/33 (CH wagging and C4−N2 stretching, together with quinoid-aromatic transformation), 34, 41, and 42 (ring stretchings combined with CH wagging, CH_3 and NH_2 bending), the electrical part is the largest. At $\lambda = \infty$, their $\Delta\beta_{\parallel}^{ZPVA}$ contributions are mostly negative for the isolated molecule, but their amplitudes decrease at smaller wavelengths. On the other hand, when accounting for the charge field, many of these contributions are negative in the static limit and become strongly positive at λ = 1064 nm. The approximate symmetry of these normal modes can be associated with those of *p*-nitroaniline (*p*NA): 8/9, 23, 32/33, 42-A_1, 34, 41-B_1, 18-B_2.[26]

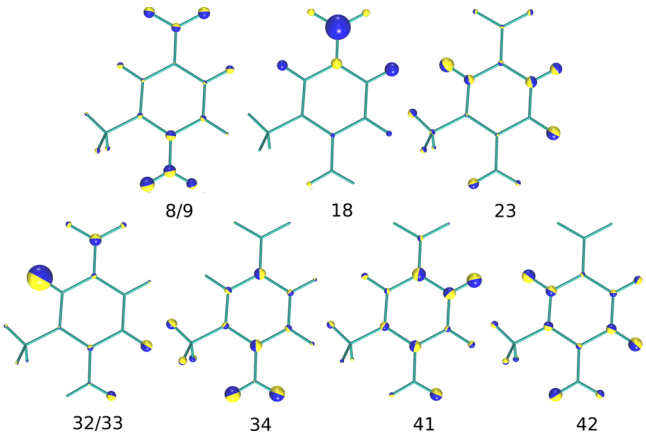

Figure 4. Sketches of the atomic displacements of the vibrational normal modes contributing mostly to the ZPVA corrections with/without a polarizing field. The direction of atomic displacements is perpendicular to the junction plane between the two hemispheres of distinct color, and their amplitudes are proportional to the radius of the sphere.

Let us now turn to analyzing the impact of the molecular ZPVA contributions, evaluated at the B3LYP/6-311++G(d,p) level, on the macroscopic electric properties. Although, upon adding the ZPVA contributions, the molecular static first hyperpolarizability decreases slightly (∼2.5%), the increase of the polarizability leads to an enhancement of both $\chi^{(1)}$ and $\chi^{(2)}$. A comparison of the electric susceptibility tensor components with and without ZPVA is given in Table 5 for molecular electronic properties evaluated at the B3LYP and CCSD levels of theory, while the effect of ZPVA corrections on the $\chi_{111}^{(2)}$ frequency dispersion is shown in Figure 5. Including ZPVA has a systematic effect of increasing $\chi^{(1)}$ and $\chi^{(2)}$, at both the B3LYP and CCSD levels as well as for both the static and dynamic quantities. So, the dynamic $\chi_{11}^{(1)}$ quantity increases by 0.10 and the difference, with respect to experiment, goes up to 10.3% and 9.4% at the B3LYP and CCSD levels of approximation, in comparison to 6.6% and 5.8% in the absence of ZPVA corrections, respectively. Moreover, upon adding ZPVA correction to the polarizability and first hyperpolarizability, the dynamic $\chi_{111}^{(2)}$ quantity increases by 12% and 11% at the B3LYP and CCSD levels, respectively. Thus, adding the ZPVA worsens the agreement with experiment at the CCSD level—because of the overestimated dressing field—whereas, at the B3LYP level, the agreement gets better, because the B3LYP method underestimates the CCSD first hyperpolarizabilities.

3.3. Geometry Effect. The full set of atomic positions obtained from PBC geometry optimizations were already determined in ref 13, so that we only remind that PBC geometry optimization leads to an overestimation of the experimental bond length alternation (0.037 Å, instead of 0.028 Å).[13] This leads to an increase of the molecular response both directly and indirectly, which also follows from the enhancement of the polarizing electric field strength. The static and dynamic (λ = 1064 nm) molecular properties at the PBC-optimized geometry are given in Tables S6 and S7 in the Supporting Information) and can be compared with those obtained at the experimental geometry (Tables S2 and S3 in the Supporting Information). In the static $\lambda = \infty$ limit, the geometry optimization leads to an increase of the α_{iso} value by ca. 2%, with respect to the values obtained at the experimental geometry. However, for the first hyperpolarizability, the situation is more complex. The correlated methods (and also the HF scheme) predict an increase of β_{tot} by ca. 9%−14%. A smaller increase is also predicted for range-corrected and M05-2X functionals: 8.5% for LC-BLYP and ca. 2.5% for CAM-B3LYP and M05-2X. On the other hand, BLYP predicts the largest decrease of 5.9%, while hybrid functionals give a decrease of ca. 2.5%. The change in β_{tot} obtained with the double hybrid functionals is close to zero. A similar trend is also observed for dynamic properties. Such differences in the geometrical dependence of the molecular responses when using wave function-based or density-based methods is typical of what was observed for the ratio between the electronic and vibrational contributions to the hyperpolarizabilities of push−pull π-conjugated systems.[58]

The static and dynamic macroscopic electric susceptibilities calculated for the optimized geometry are presented in Tables 6 and 7. The frequency dispersions of n_x and of $\chi_{111}^{(2)}$ evaluated at the HF, MP2, BLYP, B3LYP, and LC-BLYP levels are displayed for both geometries in Figures 6 and 7. The general effect of using the PBC-optimized geometry instead of the experimental

Table 5. Influence of the ZPVA Correction Estimated at the B3LYP/6-311++G(d,p) Level of Theory on the Electric Susceptibility Tensor Components and Refractive Indices Calculated at $\lambda = \infty$ and $\lambda = 1064$ nm for B3LYP and CCSD Molecular Electronic Properties[a]

method	$\chi^{(1)}_{11}$	$\chi^{(1)}_{22}$	$\chi^{(1)}_{33}$	$\chi^{(1)}_{13}$	n_x	n_y	n_z	$\chi^{(2)}_{111}$	$\chi^{(2)}_{122}$	$\chi^{(2)}_{212}$
					$\lambda = \infty$					
experiment	2.453	1.956	1.422	0.709	1.953	1.719	1.436	117.8		
B3LYP	2.757	1.915	1.448	0.861	2.045	1.707	1.422	−97.6	−6.2	
B3LYP and ZPVA	2.845	2.007	1.517	0.883	2.070	1.734	1.441	−99.2	−6.3	
CCSD	2.754	1.926	1.426	0.866	2.045	1.710	1.414	−180.0	−15.2	
CCSD and ZPVA	2.839	2.016	1.500	0.894	2.070	1.737	1.433	−185.4	−15.5	
					$\lambda = 1064$ nm					
experiment	2.804	2.000	1.521	0.883	2.063	1.732	1.439	300(75)	45(11)	
B3LYP	2.990	1.976	1.513	0.970	2.114	1.725	1.426	−274.1	−13.4	−19.6
B3LYP and ZPVA	3.094	2.074	1.587	1.000	2.143	1.753	1.445	−308.8	−14.8	−22.0
CCSD	2.967	1.983	1.485	0.966	2.108	1.727	1.417	−438.2	−32.8	−35.9
CCSD and ZPVA	3.067	2.078	1.566	1.002	2.137	1.754	1.437	−485.2	−35.1	−38.8

[a] $\chi^{(2)}$ tensor elements given in units of pm/V.

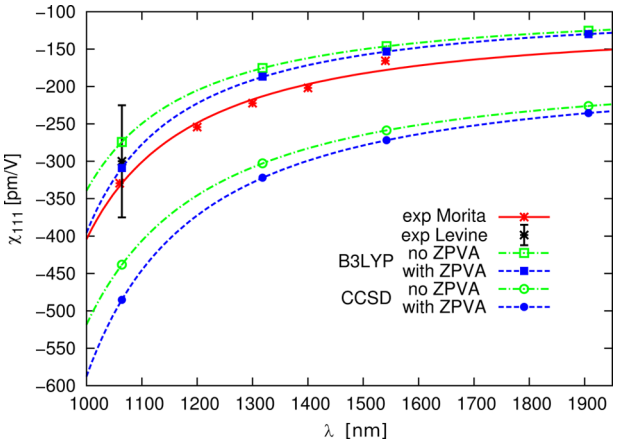

Figure 5. Influence of the B3LYP/6-311++G(d,p) ZPVA correction to the polarizability and first hyperpolarizability tensors on $\chi^{(2)}_{111}$ calculated using molecular electronic properties evaluated (i) at the B3LYP/6-311++G(d,p) level of theory with charge field and (ii) at the CCSD/6-31++G(d,p) level with dipole polarizing field.

one is to increase the molecular polarizability, especially along the polar direction, which, in turn, enhances the dominant refractive index n_x. This increase of α is observed for all methods, although it is larger for the correlated wave function and HF methods than with DFT. Much different effects are observed for the $\chi^{(2)}_{111}$ results. Although the molecular hyperpolarizability decreases for most of the DFT methods, the local field tensor effects (eq 4) dominates and the (amplitudes of the) $\chi^{(2)}$ tensor components increase. The only exception is the BLYP XC functional, for which, in the static limit, a small decrease (1%) is observed, while at $\lambda = 1064$ nm, a modest increase of ca. 1% is seen. In Figure 7, it is virtually impossible to distinguish the frequency dispersion curves corresponding to the two geometries for BLYP, as they overlap almost perfectly. The larger the amount of exact HF exchange in the functional, the larger the increase of $\chi^{(2)}$ after geometry optimization. LC-BLYP is the only functional for which the increase of $\chi^{(2)}_{111}$ due to geometry optimization is comparable to that achieved by the MP2 method. The wave function methods present the largest enhancement, which attains even 50% for CCSD. Interestingly, the double hybrid

Table 6. Influence of the Method Used To Calculate the Static ($\lambda = \infty$) Molecular Properties on the Macroscopic Electric Properties Taking into Account the Charge Field (Optimized Geometry)[a])

method	$\chi^{(1)}_{11}$	$\chi^{(1)}_{22}$	$\chi^{(1)}_{33}$	$\chi^{(1)}_{13}$	n_x	n_y	n_z	$\chi^{(2)}_{111}$	$\chi^{(2)}_{122} = \chi^{(2)}_{212}$
experiment	2.453[b]	1.956[b]	1.422[b]	0.709[b]	1.953[b]	1.719[b]	1.436[b]	117.8[c]	
HF	2.445	1.828	1.402	0.659	1.940	1.682	1.443	−72.0	−2.7
MP2	2.874	1.995	1.448	0.882	2.072	1.730	1.424	−162.0	−13.8
MP4	2.648	1.903	1.380	0.784	2.006	1.704	1.416	−135.7	−10.8
CCSD	3.050	1.991	1.472	0.981	2.126	1.729	1.415	−233.7	−19.7
CCSD*	2.840	1.953	1.431	0.872	2.063	1.718	1.419	−187.3	−15.5
BLYP	3.159	2.108	1.631	0.962	2.150	1.763	1.472	−90.3	−5.0
B3LYP	2.969	2.022	1.556	0.889	2.097	1.738	1.458	−93.7	−5.4
B98	2.934	2.010	1.545	0.873	2.087	1.735	1.457	−91.5	−5.3
LC-BLYP	2.662	1.923	1.452	0.759	2.007	1.710	1.444	−97.2	−6.5
CAM-B3LYP	2.815	1.978	1.510	0.820	2.052	1.726	1.454	−96.9	−6.1
M05	2.961	2.032	1.546	0.888	2.095	1.741	1.455	−92.9	−5.3
M05-2X	2.737	1.927	1.478	0.791	2.029	1.711	1.448	−88.3	−5.2
B2PLYP	2.911	1.949	1.455	0.905	2.084	1.717	1.422	−132.9	−9.8
mPW2PLYP	2.871	1.937	1.446	0.887	2.073	1.714	1.422	−128.3	−9.2

[a] CCSD results are obtained with uniform dipole dressing field, while CCSD* stands for simulated dressing electric field, according to eq 6 (see Section 2.2). $\chi^{(2)}$ tensor elements given in units of pm/V. [b] Data taken from ref 61 ($\angle(a,x) = 27°$). [c] Data extrapolated to $\lambda = \infty$ from ref 62.

Table 7. Influence of the Method Used To Calculate the Dynamic (λ = 1064 nm) Molecular Properties on the Macroscopic Electric Properties Taking into Account the Charge Field (Optimized Geometry)[a]

method	$\chi^{(1)}_{11}$	$\chi^{(1)}_{22}$	$\chi^{(1)}_{33}$	$\chi^{(1)}_{13}$	n_x	n_y	n_z	$\chi^{(2)}_{111}$	$\chi^{(2)}_{122}$	$\chi^{(2)}_{212}$
experiment	2.804[b]	2.000[b]	1.521[b]	0.883[b]	2.063[b]	1.732[b]	1.439[b]	300(75)[c]	45(11)[c]	
HF	2.562	1.868	1.437	0.711	1.976	1.694	1.447	−125.6	−4.0	−7.0
MP2	3.121	2.052	1.512	0.996	2.144	1.747	1.427	−462.3	−37.1	−33.1
MP4	2.867	1.956	1.438	0.884	2.071	1.719	1.420	−374.8	−28.1	−25.7
CCSD	3.340	2.060	1.547	1.116	2.208	1.749	1.419	−675.0	−49.6	−52.5
CCSD*	3.068	2.014	1.492	0.978	2.130	1.736	1.423	−482.6	−35.5	−39.3
BLYP	3.477	2.184	1.716	1.110	2.239	1.784	1.476	−327.6	−11.6	−20.6
B3LYP	3.222	2.086	1.624	1.006	2.170	1.757	1.462	−262.8	−11.4	−17.8
B98	3.173	2.072	1.610	0.984	2.156	1.753	1.461	−245.4	−10.9	−16.8
LC-BLYP	2.832	1.974	1.499	0.836	2.058	1.725	1.448	−207.4	−12.3	−15.8
CAM-B3LYP	3.020	2.035	1.567	0.914	2.112	1.742	1.458	−231.5	−12.2	−16.8
M05	3.202	2.096	1.611	0.999	2.164	1.760	1.459	−252.2	−11.0	−17.3
M05-2X	2.924	1.980	1.529	0.877	2.085	1.726	1.451	−198.9	−9.9	−14.0
B2PLYP	3.164	2.005	1.521	1.022	2.157	1.734	1.425	−381.7	−26.4	−23.7
mPW2PLYP	3.119	1.993	1.511	1.001	2.144	1.730	1.425	−366.5	−24.7	−22.4

[a]CCSD results are obtained with uniform dipole dressing field, while CCSD* stands for simulated dressing electric field, according to eq 6 (see Section 2.2). $\chi^{(2)}$ tensor elements given in units of pm/V. [b]Data taken taken from ref 61 ($\angle(a,x)$ = 27°). [c]Data taken from ref 63.

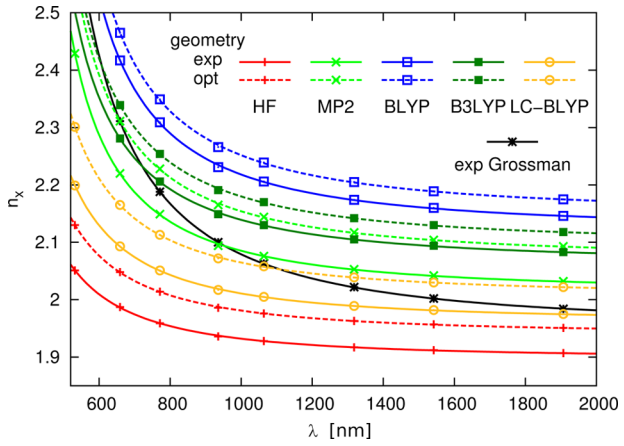

Figure 6. Frequency dispersion of the refractive index n_x as calculated with selected methods in comparison with experiment. Two geometries were employed with inclusion of the electric polarizing field at the stage of molecular properties calculations, whereas no ZPVA correction was taken into consideration.

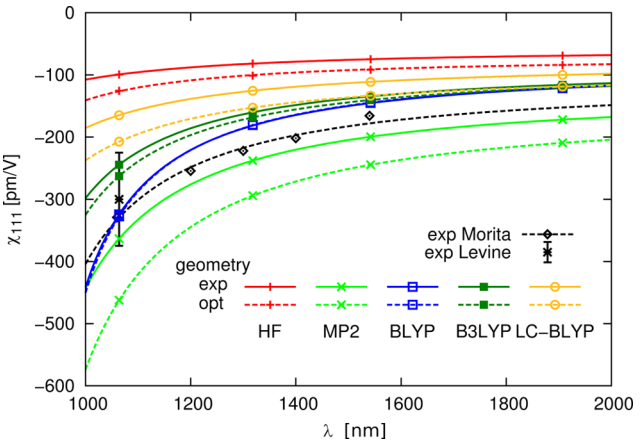

Figure 7. Frequency-dispersion of the second-order nonlinear optical susceptibility component $\chi^{(2)}_{111}$ as calculated with selected methods in comparison with experiment. Two geometries were employed with inclusion of the electric polarizing field at the stage of molecular properties calculations, whereas no ZPVA correction was taken into consideration.

functionals are, in this view, much less sensitive to a change of geometry, comparable to CAM-B3LYP and M05-2X. Concluding the current discussion, only the wave function methods may be reliable enough in discriminating between a set of available molecular geometries within the RLFT*n* approach. Moreover, using PBC-optimized geometry instead of the experimental one worsens the agreement with experiment for $\chi^{(1)}$ and $\chi^{(2)}$.

4. FURTHER DISCUSSIONS AND CONCLUSIONS

In this paper, the local field theory has been employed to calculate the linear and second-order nonlinear optical susceptibilities of the 2-methyl-4-nitroaniline (MNA) crystal, which consists of first computing the molecular properties, accounting for the dressing effects of the surroundings, and then taking into account the local field effects. Several aspects of these calculations have been tackled, in comparison with experiment. First, the effects of electron correlation have been investigated on the molecular properties and subsequently on the macroscopic responses. In particular, we have assessed the performance of a range of exchange-correlation functionals. In this case, comparisons with high-level wave function methods have also been carried out. With respect to the reference CCSD-based results, besides double hybrid functionals, the most-reliable XC functionals are LC-BLYP for the static $\chi^{(1)}$ and CAM-B3LYP (and M05-2X to lesser extent) for the dynamic $\chi^{(1)}$ but they strongly underestimate $\chi^{(2)}$. Double hybrids perform better for $\chi^{(2)}$ but not necessarily for $\chi^{(1)}$. Moreover, for the latter, the performances are quite similar to MP2, which is known to overestimate β, with respect to high-level CCSD(T) calculations[55] and, therefore, $\chi^{(2)}$. The other XC functionals with less HF exchange perform poorly with overestimations/underestimations of $\chi^{(1)}/\chi^{(2)}$, whereas the HF method leads to underestimations of both. The first-order ZPVA correction, estimated at the B3LYP level, is usually small but not negligible. Indeed, after ZPVA corrections the molecular polarizabilities and first hyperpolarizabilities increase by 2% and 5%, respectively, whereas the ZPVA effects are magnified on the macroscopic responses with enhancements of $\chi^{(1)}$ by up to 5% and of $\chi^{(2)}$ by as much as 10%−12% at λ =

dx.doi.org/10.1021/ct5001654 | J. Chem. Theory Comput. 2014, 10, 2114−2124

Table 8. Influence of the Successive Improvements of the Molecular Properties on Calculated $\chi^{(1)}$ and $\chi^{(2)}$ Tensor Components ($\lambda = \infty$)[a]

method	$\chi^{(1)}_{11}$	$\chi^{(1)}_{22}$	$\chi^{(1)}_{33}$	$\chi^{(1)}_{13}$	$\chi^{(2)}_{111}$	$\chi^{(2)}_{122}$
experiment	2.453[b]	1.956[b]	1.422[b]	0.709[b]	117.8[c]	
Experimental Geometry						
MP2 no field	2.264	1.902	1.327	0.612	−63.5	−6.2
MP2 dipole field	2.821	1.965	1.450	0.893	−165.8	−14.5
MP2 charge field	2.657	1.931	1.421	0.807	−134.3	−11.4
MP2 charge field + ZPVA (B3LYP)	2.743	2.024	1.489	0.828	−137.3	−11.8
CCSD no field	2.187	1.866	1.298	0.581	−63.0	−5.2
CCSD dipole field	2.754	1.926	1.426	0.866	−180.0	−15.2
CCSD dipole field + ZPVA (B3LYP)	2.842	2.018	1.494	0.889	−184.8	−15.7
CCSD*	2.682	1.948	1.471	0.798	−143.8	−11.6
CCSD* + ZPVA (B3LYP)	2.772	2.042	1.544	0.821	−145.1	−11.6
PBC-Optimized Geometry						
MP2 no field	2.382	1.954	1.337	0.644	−75.3	−7.8
MP2 dipole field	3.087	2.034	1.489	0.992	−202.0	−17.5
MP2 charge field	2.874	1.995	1.448	0.882	−162.0	−13.8
MP2 charge field + ZPVA (B3LYP)	2.965	2.090	1.517	0.906	−166.1	−14.2
CCSD no field	2.296	1.909	1.306	0.61	−74.3	−6.6
CCSD dipole field	3.050	1.991	1.472	0.981	−233.7	−19.7
CCSD dipole field + ZPVA (B3LYP)	3.146	2.086	1.542	1.008	−240.8	−20.4
CCSD*	2.840	1.953	1.431	0.872	−187.3	−15.5
CCSD* + ZPVA (B3LYP)	2.934	2.049	1.505	0.896	−188.7	−15.6
Geometry Optimized with Point Charges						
MP2 no field	2.264	1.918	1.335	0.612	−63.2	−6.6
MP2 charge field	2.661	1.950	1.429	0.807	−136.1	−12.3
MP2 charge field + ZPVA (B3LYP)	2.747	2.043	1.498	0.828	−139.2	−12.7

[a] $\chi^{(2)}$ tensor elements given in units of pm/V. [b] Data taken from ref 61 ($\angle(a,x) = 27°$). [c] Data extrapolated to $\lambda = \infty$ from ref 62.

Table 9. Influence of the Successive Improvements of the Molecular Properties on Calculated $\chi^{(1)}$ and $\chi^{(2)}$ Tensor Components (λ = 1064 nm)[a]

method	$\chi^{(1)}_{11}$	$\chi^{(1)}_{22}$	$\chi^{(1)}_{33}$	$\chi^{(1)}_{13}$	$\chi^{(2)}_{111}$	$\chi^{(2)}_{122}$	$\chi^{(2)}_{212}$
experiment	2.804[b]	2.000[b]	1.521[b]	0.883[b]	300(75)[c]	45(11)[c]	
Experimental Geometry							
MP2 no field	2.386	1.946	1.365	0.667	−139.3	−13.3	−12.7
MP2 dipole field	3.079	2.021	1.520	1.015	−497.6	−40.6	−35.4
MP2 charge field	2.865	1.983	1.479	0.904	−363.3	−29.4	−26.6
MP2 charge field + ZPVA (B3LYP)	2.966	2.079	1.553	0.933	−415.6	−33.7	−30.0
CCSD no field	2.274	1.907	1.328	0.618	−106.2	−8.5	−9.6
CCSD dipole field	2.967	1.983	1.485	0.966	−438.2	−32.8	−35.9
CCSD dipole field + ZPVA (B3LYP)	3.070	2.080	1.559	0.996	−483.5	−35.6	−39.3
CCSD*	2.857	2.002	1.522	0.880	−319.0	−23.1	−26.1
CCSD* + ZPVA (B3LYP)	2.963	2.102	1.602	0.910	−351.6	−24.3	−28.4
PBC-Optimized Geometry							
MP2 no field	2.522	2.001	1.377	0.706	−171.2	−17.2	−16.2
MP2 dipole field	3.398	2.099	1.568	1.136	−646.7	−51.8	−44.2
MP2 charge field	3.121	2.052	1.512	0.996	−462.3	−37.1	−33.1
MP2 charge field + ZPVA (B3LYP)	3.230	2.152	1.588	1.028	−533.8	−42.9	−37.6
CCSD no field	2.399	1.955	1.338	0.654	−131.1	−11.1	−12.5
CCSD dipole field	3.340	2.060	1.547	1.116	−675.0	−49.6	−52.5
CCSD dipole field + ZPVA (B3LYP)	3.455	2.160	1.624	1.152	−747.8	−54.2	−57.3
CCSD*	3.068	2.014	1.492	0.978	−482.6	−35.5	−39.3
CCSD* + ZPVA (B3LYP)	3.180	2.116	1.572	1.011	−519.1	−36.8	−41.9
Geometry Optimized with Point Charges							
MP2 no field	2.392	1.964	1.375	0.670	−140.9	−14.3	−13.5
MP2 charge field	2.886	2.005	1.492	0.913	−387.6	−33.1	−29.6
MP2 charge field + ZPVA (B3LYP)	2.987	2.103	1.566	0.942	−440.2	−37.8	−33.1

[a] $\chi^{(2)}$ tensor elements given in units of pm/V. [b] Data taken from ref 61 ($\angle(a,x) = 27°$). [c] Data taken from ref 63.

1064 nm. The choice of a geometry is also a key factor for accurate prediction of the susceptibilities, particularly for push−pull π-conjugated compounds such as MNA. So, the geometry optimized using periodic boundary conditions is characterized by an overestimated bond length alternation, which gives larger molecular properties and even larger macroscopic responses, because of the local field factor amplification effects. Improvements of the $\chi^{(1)}$ and $\chi^{(2)}$ values as calculated from optimized geometries could also be achieved by performing PBC geometry optimizations at a higher level of approximation or by using a more appropriate XC functional. However, this is a subtle issue, as illustrated in ref 59, where, for quasilinear π-conjugated chains containing from two to six unit cells, no single XC functional emerges as uniformly accurate for all oligomeric series and chain lengths. Moreover, considering recent data on push−pull polyenes,[60] B3LYP could either underestimate (push−pull polyenes) or overestimate (MNA, present work) the BLA, demonstrating that HF exchange could play a dual role.

Based on these results and analysis, additional calculations of $\chi^{(1)}$ and $\chi^{(2)}$ have been performed and the results are provided in Tables 8 and 9 for the static and dynamic quantities, respectively. These tables aim at monitoring the convergence of the $\chi^{(1)}$ and $\chi^{(2)}$ predictions, with respect to experiment, by accounting for the complementary effects of (i) the dressing field within successive approximations, (ii) the ZPVA correction, and (iii) the geometry. Only MP2-based and CCSD-based results are presented because they provide the best molecular responses. Our best estimates based on experimental geometries, charge dressing field, ZPVA correction, and CCSD molecular properties lead to an overestimation of $\chi^{(1)}$ by 12% in the static limit and 7% at λ = 1064 nm. For $\chi^{(2)}$, the difference with respect to experiment is satisfactory and of the order of one standard deviation. An attempt to optimize the molecular geometry with the use of a point charge field, necessary to calculate ZPVA corrections in the presence of the dressing field, has demonstrated that it provides geometries in close agreement to experiment and, therefore, similar $\chi^{(1)}$ and $\chi^{(2)}$ responses. This demonstrates the potential of this optimization procedure when crystal structures of high precision are lacking. On this basis, the local field theory can be used for screening the linear and nonlinear optical properties of molecular crystals in view of designing materials for photonics devices.

■ ASSOCIATED CONTENT

Supporting Information

Mulliken atomic populations; molecular (hyper)polarizability calculation results; dipole moments and electric field obtained with MP2 and CCSD calculations; normal modes contributions to ZPVA corrections. This material is available free of charge via the Internet at http://pubs.acs.org.

■ AUTHOR INFORMATION

Corresponding Authors

*E-mail: seidler@chemia.uj.edu.pl.
*E-mail: benoit.champagne@unamur.be.

Notes

The authors declare no competing financial interest.

■ ACKNOWLEDGMENTS

This research was supported in part by PL-Grid Infrastructure as well as by the Belgium government (IUAP No. P7/05, Functional Supramolecular Systems). T.S. acknowledges the support from a project operated within the Foundation for Polish Science MPD Programme (cofinanced by the EU European Regional Development Fund), as well as the financial support of IUAP No. P7/05. The calculations were performed on the Technological Platform of High-Performance Computing of the Consortium des Equipements de Calcul Intensif, for which we gratefully acknowledge the financial support of the FNRS-FRFC (Convention Nos. 2.4.617.07.F and 2.5020.11), and of the University of Namur.

■ REFERENCES

(1) Champagne, B.; Bishop, D. M. *Adv. Chem. Phys.* **2003**, *126*, 41−92.
(2) Kwon, O.-P.; Jazbinsek, M.; Seo, J.-I.; Choi, E. Y.; Yun, H.; Brunner, F. D. J.; Lee, Y. S.; Günter, P. *J. Chem. Phys.* **2009**, *130*, 134708.
(3) Jayatilaka, D.; Munshi, P.; Turner, M. J.; Howard, J. A. K.; Spackman, M. A. *Phys. Chem. Chem. Phys.* **2009**, *11*, 7209−7218.
(4) Kim, J.; Kwon, O.-P.; Jazbinsek, M.; Park, Y. C.; Seo, J.-I.; Lee, Y. S. *J. Phys. Chem. C* **2011**, *115*, 23535−23542.
(5) Ségerie, A.; Castet, F.; Kanoun, M. B.; Plaquet, A.; Liégeois, V.; Champagne, B. *Chem. Mater.* **2011**, *23*, 3993−4001.
(6) Suponitsky, K. Y.; Masunov, A. *J. Chem. Phys.* **2013**, *139*, 094310.
(7) Chemla, D.; Oudar, J.; Jerphagnon, J. *Phys. Rev. B* **1975**, *12*, 4534−4546.
(8) Zyss, J.; Oudar, J. *Phys. Rev. A* **1982**, *26*, 2028−2048.
(9) Munn, R. W. *Chem. Phys.* **1980**, *50*, 119.
(10) Hurst, M.; Munn, R. W. *J. Mol. Electron.* **1986**, *2*, 35.
(11) Reis, H.; Papadopoulos, M. G.; Munn, R. W. *J. Chem. Phys.* **1998**, *109*, 6828−6838.
(12) Reis, H.; Papadopoulos, M. G.; Calaminici, P.; Jug, K.; Köster, A. M. *Chem. Phys.* **2000**, *261*, 359−371.
(13) Seidler, T.; Stadnicka, K.; Champagne, B. *J. Chem. Phys.* **2013**, *139*, 114105.
(14) Champagne, B.; Perpète, E. A.; Jacquemin, D.; van Gisbergen, S. J. A.; Baerends, E. J.; Soubra-Ghaoui, C.; Robins, K.; Kirtman, B. *J. Phys. Chem. A* **2000**, *104*, 4755.
(15) Bulat, F. A.; Toro-Labbé, A.; Champagne, B.; Kirtman, B.; Yang, W. *J. Chem. Phys.* **2005**, *123*, 014319.
(16) Sekino, H.; Maeda, Y.; Kamiya, M.; Hirao, K. *J. Chem. Phys.* **2005**, *123*, 014107.
(17) Jacquemin, D.; Perpète, E. A.; Medved, M.; Scalmani, G.; Frisch, M. J.; Kobayashi, R.; Adamo, C. *J. Chem. Phys.* **2007**, *126*, 191108.
(18) Suponitsky, K. Y.; Tafur, S.; Masunov, A. E. *J. Chem. Phys.* **2008**, *129*, 044109.
(19) Borini, S.; Limacher, P. A.; Luthi, H. P. *J. Chem. Phys.* **2010**, *131*, 124105.
(20) Vila, F. D.; Strubbe, D. A.; Takimoto, Y.; Andrade, X.; Rubio, A.; Louie, S. G.; Rehr, J. J. *J. Chem. Phys.* **2010**, *133*, 034111.
(21) Karamanis, P.; Marchal, R.; Carbonnière, P.; Pouchan, C. *J. Chem. Phys.* **2011**, *135*, 044511.
(22) Kirtman, B.; Lacivita, V.; Dovesi, R.; Reis, H. *J. Chem. Phys.* **2011**, *135*, 154101.
(23) Castet, F.; Champagne, B. *J. Chem. Theory Comput.* **2012**, *8*, 2044−2052.
(24) Bulik, I. W.; Zalesny, R.; Bartkowiak, W.; Luis, J. M.; Kirtman, B.; Scuseria, G. E.; Avramopoulos, A.; Reis, H.; Papadopoulos, M. G. *J. Comput. Chem.* **2013**, *34*, 1775.
(25) Quinet, O.; Kirtman, B.; Champagne, B. *J. Chem. Phys.* **2003**, *118*, 505.
(26) Quinet, O.; Champagne, B.; Kirtman, B. *J. Mol. Struct. (THEOCHEM)* **2003**, *633*, 199−207.

(27) Torrent-Sucarrat, M.; Sola, M.; Duran, M.; Luis, J. M.; Kirtman, B. *J. Chem. Phys.* **2004**, *120*, 6346.
(28) Luis, J. M.; Torrent-Sucarrat, M.; Christiansen, O.; Kirtman, B. *J. Chem. Phys.* **2007**, *127*, 084118.
(29) Bast, R.; Saue, T.; Hendriksson, J.; Norman, P. *J. Chem. Phys.* **2009**, *130*, 024109.
(30) Bast, R.; Thorvaldsen, A. J.; Ringholm, M.; Ruud, K. *Chem. Phys.* **2009**, *356*, 177−186.
(31) Naves, E. S.; Castro, M. A.; Fonseca, T. L. *J. Chem. Phys.* **2011**, *134*, 054315.
(32) Pecul, M.; Pawlowski, F.; Jorgensen, P.; Hättig, C. *J. Chem. Phys.* **2006**, *124*, 114101.
(33) Hammond, J. R.; Kowalski, K. *J. Chem. Phys.* **2009**, *130*, 194108.
(34) Hanauer, M.; Köhn, H. *J. Chem. Phys.* **2009**, *131*, 124118.
(35) Castet, F.; Bogdan, E.; Plaquet, A.; Ducasse, L.; Champagne, B.; Rodriguez, V. *J. Chem. Phys.* **2012**, *136*, 024506.
(36) Hurst, M.; Munn, R. W. *J. Mol. Electron.* **1986**, *2*, 43.
(37) Munn, R. W. *Mol. Phys.* **1988**, *64*, 1−20.
(38) Whitten, A. E.; Turner, P.; Klooster, W. T.; Piltz, R. O.; Spackman, M. A. *J. Phys. Chem. A* **2006**, *110*, 8763−8776.
(39) Dovesi, R.; Orlando, R.; Civalleri, B.; Roetti, C.; Saunders, V. R.; Zicovich-Wilson, C. M. *Z. Kristallogr.* **2005**, *220*, 571.
(40) Dovesi, R.; Saunders, V. R.; Roetti, C.; Orlando, R.; Zicovich-Wilson, C. M.; Pascale, F.; Civalleri, B.; Doll, K.; Harrison, N. M.; Bush, I. J.; D'Arco, P.; Llunell, M. *CRYSTAL09 User's Manual*; University of Torino: Torino, Italy, 2009.
(41) Frisch, M. J.; Trucks, G. W.; Schlegel, H. B.; Scuseria, G. E.; Robb, M. A.; Cheeseman, J. R.; Scalmani, G.; Barone, V.; Mennucci, B.; Petersson, G. A.; Nakatsuji, H.; Caricato, M.; Li, X.; Hratchian, H. P.; Izmaylov, A. F.; Bloino, J.; Zheng, G.; Sonnenberg, J. L.; Hada, M.; Ehara, M.; Toyota, K.; Fukuda, R.; Hasegawa, J.; Ishida, M.; Nakajima, T.; Honda, Y.; Kitao, O.; Nakai, H.; Vreven, T.; Montgomery, Jr., J. A.; Peralta, J. E.; Ogliaro, F.; Bearpark, M.; Heyd, J. J.; Brothers, E.; Kudin, K. N.; Staroverov, V. N.; Kobayashi, R.; Normand, J.; Raghavachari, K.; Rendell, A.; Burant, J. C.; Iyengar, S. S.; Tomasi, J.; Cossi, M.; Rega, N.; Millam, J. M.; Klene, M.; Knox, J. E.; Cross, J. B.; Bakken, V.; Adamo, C.; Jaramillo, J.; Gomperts, R.; Stratmann, R. E.; Yazyev, O.; Austin, A. J.; Cammi, R.; Pomelli, C.; Ochterski, J. W.; Martin, R. L.; Morokuma, K.; Zakrzewski, V. G.; Voth, G. A.; Salvador, P.; Dannenberg, J. J.; Dapprich, S.; Daniels, A. D.; Farkas, O.; Foresman, J. B.; Ortiz, J. V.; Cioslowski, J.; Fox, D. J. *Gaussian 09 Revision D.01*; Gaussian, Inc.: Wallingford, CT, 2009.
(42) Sekino, H.; Bartlett, R. J. *J. Chem. Phys.* **1991**, *94*, 3665−3669.
(43) Helgaker, T.; Coriani, S.; Jorgensen, P.; Kristensen, K.; Olsen, J.; Ruud, K. *Chem. Rev.* **2012**, *112*, 543−631.
(44) Aidas, K.; Angeli, C.; Bak, K. L.; Bakken, V.; Bast, R.; Boman, L.; Christiansen, O.; Cimiraglia, R.; Coriani, S.; Dahle, P.; Dalskov, E. K.; Ekström, U.; Enevoldsen, T.; Eriksen, J. J.; Ettenhuber, P.; Fernńdez, B.; Ferrighi, L.; Fliegl, H.; Frediani, L.; Hald, K.; Halkier, A.; Hättig, C.; Heiberg, H.; Helgaker, T.; Hennum, A. C.; Hettema, H.; Hjertenæs, E.; Høst, S.; Høyvik, I.-M.; Iozzi, M. F.; Jansik, B.; Jensen, H. J. A.; Jonsson, D.; Jørgensen, P.; Kauczor, J.; Kirpekar, S.; Kjærgaard, T.; Klopper, W.; Knecht, S.; Kobayashi, R.; Koch, H.; Kongsted, J.; Krapp, A.; Kristensen, K.; Ligabue, A.; Lutnæs, O. B.; Melo, J. I.; Mikkelsen, K. V.; Myhre, R. H.; Neiss, C.; Nielsen, C. B.; Norman, P.; Olsen, J.; Olsen, J. M. H.; Osted, A.; Packer, M. J.; Pawlowski, F.; Pedersen, T. B.; Provasi, P. F.; Reine, S.; Rinkevicius, Z.; Ruden, T. A.; Ruud, K.; Rybkin, V.; Salek, P.; Samson, C. C. M.; de Merás, A. S.; Saue, T.; Sauer, S. P. A.; Schimmelpfennig, B.; Sneskov, K.; Steindal, A. H.; Sylvester-Hvid, K. O.; Taylor, P. R.; Teale, A. M.; Tellgren, E. I.; Tew, D. P.; Thorvaldsen, A. J.; Thøgersen, L.; Vahtras, O.; Watson, M. A.; Wilson, D. J. D.; Ziolkowski, M.; Ågren, H. *WIREs Comput. Mol. Sci.*.
(45) *DALTON2011, a molecular electronic structure program (2011)*; http://www.daltonprogram.org, accessed Feb. 1, 2014.
(46) Fedorovsky, M. PyVib2, a program for analyzing vibrational motion and vibrational spectra; http://pyvib2.sourceforge.net, accessed Feb. 1, 2014.
(47) Becke, A. D. *J. Chem. Phys.* **1993**, *98*, 5648.
(48) Lee, C.; Yang, W.; Parr, R. G. *Phys. Rev. B* **1988**, *37*, 785.
(49) Becke, A. D. *Phys. Rev. A* **1988**, *38*, 3098.
(50) Schmider, H. L.; Becke, A. D. *J. Chem. Phys.* **1998**, *108*, 9624.
(51) Zhao, Y.; Schultz, N. E.; Truhlar, D. G. *J. Chem. Phys.* **2005**, *123*, 161103.
(52) Iikura, H.; Tsuneda, T.; Yanai, T.; Hirao, K. *J. Chem. Phys.* **2001**, *115*, 3540−3544.
(53) Yanai, T.; Tew, D. P.; Handy, N. C. *Chem. Phys. Lett.* **2004**, *393*, 51−57.
(54) Zhao, Y.; Schultz, N. E.; Truhlar, D. G. *J. Chem. Theory Comput.* **2006**, *2*, 364.
(55) de Wergifosse, M.; Champagne, B. *J. Chem. Phys.* **2011**, *134*, 074113.
(56) Grimme, S. *J. Chem. Phys.* **2006**, *124*, 034108.
(57) Schwabe, T.; Grimme, S. *Phys. Chem. Chem. Phys.* **2006**, *8*, 4398.
(58) Jacquemin, D.; Champagne, B.; Perpète, E. A.; Luis, J. M.; Kirtman, B. *J. Phys. Chem. A* **2001**, *105*, 9748−9755.
(59) Jacquemin, D.; Adamo, C. J. *J. Chem. Theory Comput.* **2011**, *7*, 369−376.
(60) Nénon, S.; Champagne, B. *J. Chem. Phys.* **2013**, *138*, 204107.
(61) Grossman, C. H.; Garito, A. F. *Mol. Cryst. Liq. Cryst.* **1989**, *168*, 255−267.
(62) Morita, R.; Kondo, T.; Kaneda, Y.; Sugihashi, A.; Ogasawara, N.; Umegaki, S.; Ito, R. *Jpn. J. Appl. Phys.* **1988**, *27*, L1131−L1133.
(63) Levine, B. F.; Bethea, C. G.; Thurmond, C. D.; Lynch, R. T.; Bernstein, J. L. *J. Appl. Phys.* **1979**, *50*, 2523.